ADVANCED MATERIALS INTERFACES
www.advmatinterfaces.de

A Multimodal Study on the Unique Sensing Behavior of a Guest@Metal-Organic Framework Material for the Detection of Volatile Acetone

*Annika F. Möslein, Mario Gutiérrez, Kirill Titov, Lorenzo Donà, Bartolomeo Civalleri, Mark D. Frogley, Gianfelice Cinque, Svemir Rudić, and Jin-Chong Tan**

Owing to their unique functionalities and tailorable properties that are unattainable in conventional materials, metal-organic frameworks (MOFs) have emerged as candidate materials for next-generation chemical sensors and optoelectronics. For instance, the ZnQ@OX-1 composite material, comprising a light-emitting guest encapsulated in the pores of the OX-1 framework, affords excellent sensing performance: a visible color change upon exposure to volatile acetone. In this work, a multimodal study on the exceptional vapochromism of this composite material using high-resolution spectroscopy techniques based on inelastic neutron scattering and synchrotron radiation is presented, supported by density functional theory calculations. While FTIR spectroscopy in the far-IR and mid-IR regions reveals the underlying interactions between ZnQ, OX-1, and acetone, the limit of detection at 50 ppm is determined through in situ gas dosing experiments using fluorescence spectroscopy. In addition, in situ gas dosing on the single crystal level is achieved with near-field infrared nanospectroscopy.

1. Introduction

The growing challenges of monitoring air pollution, industrial gas leakage, food safety, and personal health require chemical sensors with high sensitivity towards toxic gases and volatile organic compounds (VOCs).[1] In the medical sector, for instance, chemical sensors are used for the detection of glucose levels or electrolytes in human blood.[2] A noninvasive solution to detect low concentrations of VOCs in exhaled human breath does not yet exist, even if these biomarkers can be leveraged for early diagnosis and health monitoring.[3–5] In fact, this problem can be solved through the design of novel sensing technologies that harness the unique properties of metal-organic framework (MOF) materials.[6] Self-assembled from metal and organic building blocks and crystallizing in extended coordination networks, MOFs feature structural diversity, tailorability, high porosity, large surface area, and adsorption affinities, which offer unparalleled advantages for sensing applications.[1,7,8] First, selectivity can be achieved through size exclusion and specific host–guest interactions offered by their tunable pore size and functionalized binding sites. Secondly, the high porosity and large surface area of MOFs not only facilitate reversible uptake and release, but also accumulate the targeted analyte inside the pores for enhanced adsorption, and sensitivity, accordingly.

Inspired by the need for high-precision sensors, and the potential of MOF materials, several MOF-based devices have been developed to address the challenge of detecting small amounts of volatile acetone, summarized in Table S2 in the Supporting Information, as a non-invasive alternative for blood glucose measurements. In particular, metal-oxide systems that are prepared using MOFs as precursors can achieve sub-ppm limits of detection based on changes in resistance when acetone is adsorbed in the surface layer.[9–13] However, their high operating temperatures (>250 °C) seriously hinder their application in portable devices. Other MOF-based sensors, with sensitivity at room temperature, rely on changes in mechanical properties or capacitance upon exposure to acetone; these are however limited by the high concentration of the analyte required for detection, or slow response time, respectively.[14,15]

A. F. Möslein, M. Gutiérrez, K. Titov, G. Cinque, J.-C. Tan
Multifunctional Materials and Composites (MMC) Laboratory
Department of Engineering Science
University of Oxford
Parks Road, Oxford OX1 3PJ, UK
E-mail: jin-chong.tan@eng.ox.ac.uk
L. Donà, B. Civalleri
Dipartimento di Chimica
Università di Torino
Via P. Giuria 5, Torino 10125, Italy
M. D. Frogley, G. Cinque
Diamond Light Source
Harwell Campus
Chilton, Oxford OX11 0DE, UK
S. Rudić
STFC Rutherford Appleton Laboratory
ISIS Neutron and Muon Source
Chilton, Didcot OX11 0QX, UK

The ORCID identification number(s) for the author(s) of this article can be found under https://doi.org/10.1002/admi.202201401.

DOI: 10.1002/admi.202201401

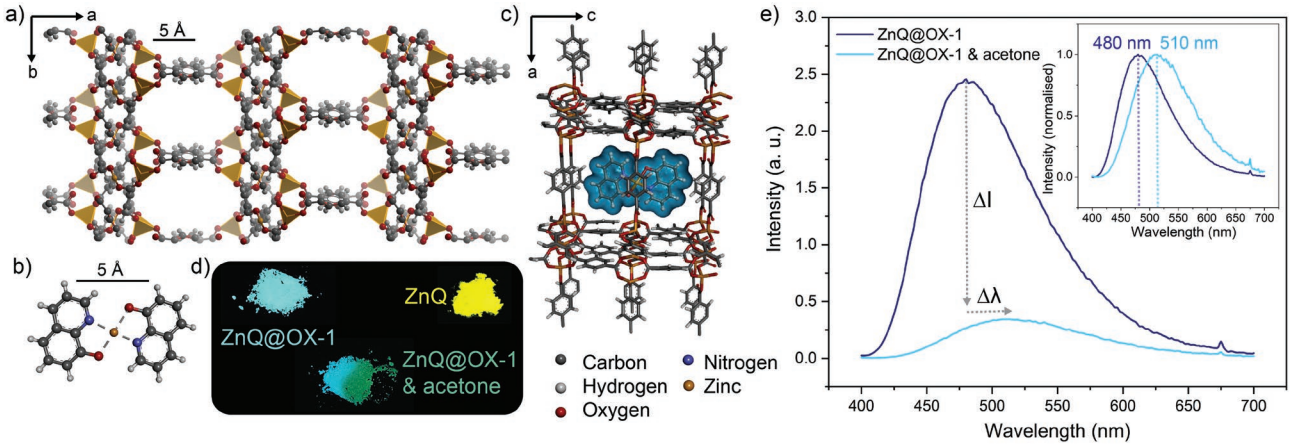

Figure 1. The ZnQ@OX-1 system. a) Structure of OX-1. b) Structure of ZnQ. c) Schematic of ZnQ encapsulated in the pores of OX-1. d) Photos of the samples under UV light (365 nm). e) Emission spectrum of ZnQ@OX-1 when exposed to acetone.

Instead, leveraging the luminescent properties is a promising strategy to design MOF-based sensor devices for the detection of gases: for instance, fluorescent quenching can be observed in the presence of acetone due to the overlap of its absorption band with the characteristic emission of the MOF.[16,17] However, because a decrease in emission intensity (or turn-off behavior) could also stem from photodegradation, or other phenomena, a shift in emission is a simpler way of detection. Such vapochromic behavior, which describes a visible color change when exposed to a gaseous analyte, is a promising way for signal transduction in optical sensors, and yet, this phenomenon is unattainable in most MOF materials. Few exemptions do however exist: the luminescent octahedron@ZIF-8 composite material exhibits a visible color change under UV irradiation when exposed to acetone for more than 15 min.[18] An even faster response (within seconds) is achieved by the "OX-1" framework, a zinc-based MOF with 1,4-benzenedicarboxylic acid (BDC) as the organic linker.[19] Only the confinement of the luminescent guest zinc(II) bis(8-hydroxyquinoline) (ZnQ) inside the pore channels of the host framework leads to the opto-chemically responsive ZnQ@OX-1 complex (**Figure 1**a–c). When subjected to UV radiation, the pristine ZnQ complex, where two 8-hydroxyquinoline (8HQ) aromatic molecules are coordinated to a single Zn center, emits an intense yellow light, or if the molecules are isolated in solution, a green light.[20,21] The ZnQ@OX-1 complex, however, exhibits an emission of blue light (480 nm), which, upon exposure to acetone, changes to a green emission (510 nm), as shown in Figure 1d. This shift in maximum emission wavelength is accompanied by quenching of emission intensity in the macroscopic scale, as the signal is decreased by one order of magnitude (Figure 1e). Hence, it is the unique photochromism, or in other words, its ability to change luminescent color in the presence of volatile acetone, that renders ZnQ@OX-1 such a promising candidate for bespoke application. Of course, solvatochromism, which describes a change in emission (or color) when subjected to different solvents, is a well-known phenomenon in MOFs, however, the fast (approximately seconds), visible response of the ZnQ@OX-1 complex to gaseous acetone is hitherto unique.[18,22,23] And yet, even if the ability of the material to sense volatile acetone has been demonstrated with a proof-of-concept device,[19] little is known about the underlying sensing mechanism. To address this challenge, we use a multimodal approach to unravel the physical and chemical interactions that are responsible for the unique gas sensing behavior. Herein, we employ spectroscopy techniques ranging from near-field and conventional Fourier transform infrared spectroscopy (FTIR) to large-scale facilities such as synchrotron-radiation based FTIR and inelastic neutron scattering (INS); all these empirical observations are further corroborated by density functional theory calculations. As a result, we acquire a thorough understanding of the sensing mechanism itself, which holds the key to tune the material further for enhanced sensing performance towards application.

2. Results and Discussions

2.1. Inelastic Neutron Scattering

Employing the TOSCA spectrometer[24] at ISIS Neutron and Muon Spallation Source, we performed inelastic neutron scattering (INS) measurements to unravel the conformational changes in the framework upon guest encapsulation and subsequent exposure to acetone. Herein, each sample was probed at 10 K for several hours. As a reference, we measured the pristine OX-1 material which does not possess any sensing abilities. When exposed to acetone, all additional peaks emerging in the INS spectrum can directly be assigned to acetone peaks and thus, the resulting spectrum is simply a superposition of the two spectra associated with pristine OX-1 and acetone, respectively, instead of indicating chemical changes (**Figure 2**a). Only in the low-energy region, the sharp peaks of pristine acetone are broadened, since, instead of crystallizing at low temperatures, the acetone molecules are isolated in the pores of the framework resulting in the loss of long-range order. In general, the modes are unaffected, and it is the lack of interactions between OX-1 and the analyte that explains why the material does not respond to the presence of acetone. However, if ZnQ is encapsulated in the framework material, we observe salient changes in the INS spectrum compared to pristine OX-1 (Figure 2b). While the presence of most peaks can be linked with peaks of either ZnQ or OX-1, such as the additional peaks at 190 or 590 cm^{-1},

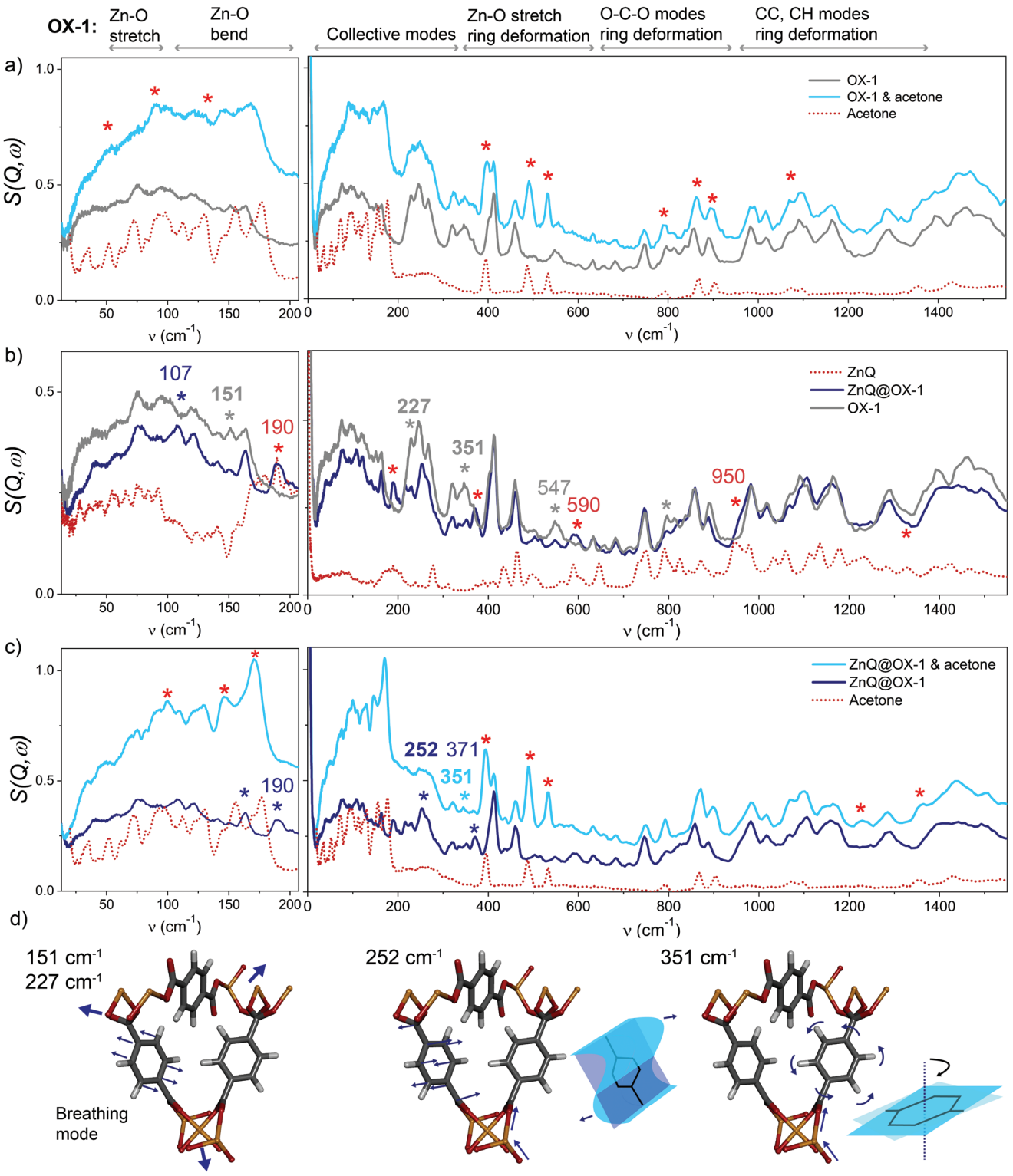

Figure 2. Inelastic neutron scattering (INS) spectra of ZnQ@OX-1 systems (scaled by mass). a) INS spectra of OX-1 before and during exposure to acetone compared with pristine acetone, reproduced from S.F. Parker, ISIS Facility, Chilton, UK. b) INS spectra of ZnQ@OX-1 and pristine host and guest materials. The broadband spectrum of ZnQ was scaled down for better comparison. c) ZnQ@OX-1 before and during exposure to acetone. d) Illustration of key vibrational modes of OX-1 affected by guest encapsulation.

or the shoulder at ≈950 cm^{-1} (all assigned to the ZnQ guest), a few changes which differ from simple superposition can be discovered. For instance, an additional peak at 107 cm^{-1} appears in a region where we observe deformation of the O—Zn—O groups (Figure 2b), as derived from density functional theory calculations (see Table S3 in Supporting Information). This

indicates structural changes and stronger O—Zn—O coordination, perhaps due to the interactions with the ZnQ complex. Meanwhile, the intensities of the peaks at 151, 227, 351 and 547 cm^{-1}, associated with pristine OX-1, are reduced, especially in relation to nearby peaks (Figure 2b). The modes at 151 and 227 cm^{-1} are ascribed to symmetric and asymmetric stretches of the Zn—O bonds resulting in out-of-plane deformations of the ring, which, consequently, trigger breathing-like modes of the pore. The two vibrations at 351 and 547 cm^{-1} that are associated with an asymmetric stretch of the Zn—O bond cause in-plane deformations of the ring, such as rotations. Significantly, the reduced intensity of these four "bulky" modes indicates their hindrance due to guest encapsulation.

These observed changes cannot simply be explained by superposition of the INS spectra of the pristine materials and are therefore a strong indicator for interactions between the luminescent guest and host framework in the ZnQ@OX-1 system. Interestingly, when the resulting ZnQ@OX-1 complex is then exposed to acetone, precisely these vibrational bands are among the ones that exhibit noticeable change, even if, at first glance, the spectrum seems to be the sum of the peaks of ZnQ@OX-1 and acetone. A close look reveals that the vibrational band at 190 cm^{-1}, associated with the ZnQ guest molecule, has reduced intensity in the presence of acetone. Similarly, the intensities of the peak at 351 cm^{-1}, which is characteristic for OX-1 but is reduced in the host–guest system, and the one at 371 cm^{-1} change in relation to each other upon exposure to acetone. In addition, the shape of the vibrational band at 252 cm^{-1} (Zn–O asymmetric stretch and tilting of the ring) is broadened, perhaps due to masking by the acetone peak (Figure 2c,d). Given that most spectral variations differ from superposition of the INS spectra of ZnQ@OX-1 and acetone, actual chemical and structural changes that are responsible for the unique sensing behavior, occur in the framework.

2.2. Synchrotron-Based FTIR Spectroscopy

To address these changes that are so crucial to understanding the mechanism itself, we performed density functional theory (DFT) calculations and (synchrotron-radiation) SR-FTIR at the MIRIAM beamline B22 at the Diamond Light Source (Oxfordshire, UK). The main advantage of the latter is that we can measure the full broadband spectrum (far-IR from 40–600 cm^{-1}, and mid-IR from 400 to 2000 cm^{-1}). Herein, we employed the Bruker Vertex FTIR spectrometer under vacuum with two different beam splitters (Mylar and KBr), as well as a bolometer and a built-in detector to measure the far-IR and mid-IR regions, respectively. Only the combination with DFT simulation however can attribute the physical vibrations with the observed peaks, therefore, we performed frequency calculations of OX-1 with the CRYSTAL17 DFT code.[25,26] Because the PBEsol0-3c composite method has recently emerged as a cost-effective way to simulate MOF materials, it was used in this work to provide functionals with basis sets for each of the 202 atoms per unit cell.[27–31] The continuous IR spectrum was obtained by fitting the calculated frequencies with Lorentzian peak shapes with a FWHM of 10 cm^{-1}. As shown in **Figure 3**a, a good match between theory and empirically measured IR spectrum is achieved. Crucially, in the far-IR region, we can observe lattice vibrations, or so-called collective Terahertz modes, which are inherently linked with structural vibrations of the entire framework, while vibrations of specific functional groups are registered in the mid-IR region.

Considering the full broadband spectrum thus reveals both structural and chemical information. For instance, the low-energy or Terahertz region encompasses lattice dynamics where key vibrational modes trigger channel-opening or shearing modes that can underpin physical phenomena ranging from enhanced gas uptake to structural instabilities.[32–34] Below 270 cm^{-1}, vibrational modes of the Zn—O with a change of angle between the bonds introduce structural deformations of the pore and channels, for instance by causing a rotation of the entire linker units. Stretching vibrations of the metal clusters, on the other hand, are prevalent in the region between 270 and 470 cm^{-1}. Even if the Zn atoms are involved in the asymmetric stretching modes observed above 470 cm^{-1} and below 700 cm^{-1}, they remain fixed and instead, in-phase ring deformations are triggered. Accordingly, in-phase and out-of-phase ring deformations are observed in the region of 700–1000 cm^{-1}, more specifically caused by stretching modes of the O—C—O groups below 850 cm^{-1}. Vibrational modes associated with the stretching of C—C bonds and scissoring (or rocking) of the C—H groups appear below 2000 cm^{-1}, while peaks above can be attributed to stretching modes of the C—H bonds. It is worth mentioning that a complete assignment of the vibrational modes of OX-1 can be found in the Supporting Information (see Table S3).

Upon exposure to acetone, OX-1 does not reveal any significant spectral changes (Figure 3a). One might argue that the general intensity is increased in the far-IR region and decreased in the mid-IR region; however, this feature is a bulk shift in intensity rather than spectral changes of individual peaks. It is the encapsulation of ZnQ in OX-1 that leads to spectral changes which cannot simply be explained by the coexistence of guest and host material, as already indicated in the INS spectra. Instead, the host–guest interactions might in fact alter the chemical environment, or even the structural lattice as a whole. This hypothesis can be confirmed by SR-FTIR measurements when comparing two different synthetic routes. First, we encapsulated commercially available ZnQ in the OX-1 framework (termed "ZnQ@OX-1 commercial"). Interestingly, albeit unveiling the same spectral features as OX-1 (Figure 3b), this synthetic route leads to a material without any sensing abilities, already emitting green light (Figure S14, Supporting Information). The second approach involves a one-pot synthesis, where ZnQ and OX-1 form simultaneously from the reactants zinc nitrate hexahydrate, 1,4-benzenedicarboxylate (BDC) linker, and 8-hydroxyquinoline (8HQ). However, the resulting ZnQ@OX-1 system exhibits significant spectral deviations from the pristine OX-1 framework material, in particularly in the far-IR region (Figure 3b). This is precisely where collective modes are prevalent, and the strong changes indicate that indeed, structural changes, remaining *N,N*-dimethylformamide (DMF) molecules from the synthesis, or even defects occur in the OX-1 framework when ZnQ is synthesized and confined in the same reaction. In fact, these findings can explain previously reported variations in the PXRD patterns of OX-1 and ZnQ@OX-1.[19] Similarly, actual chemical interactions emerge between the framework, ZnQ

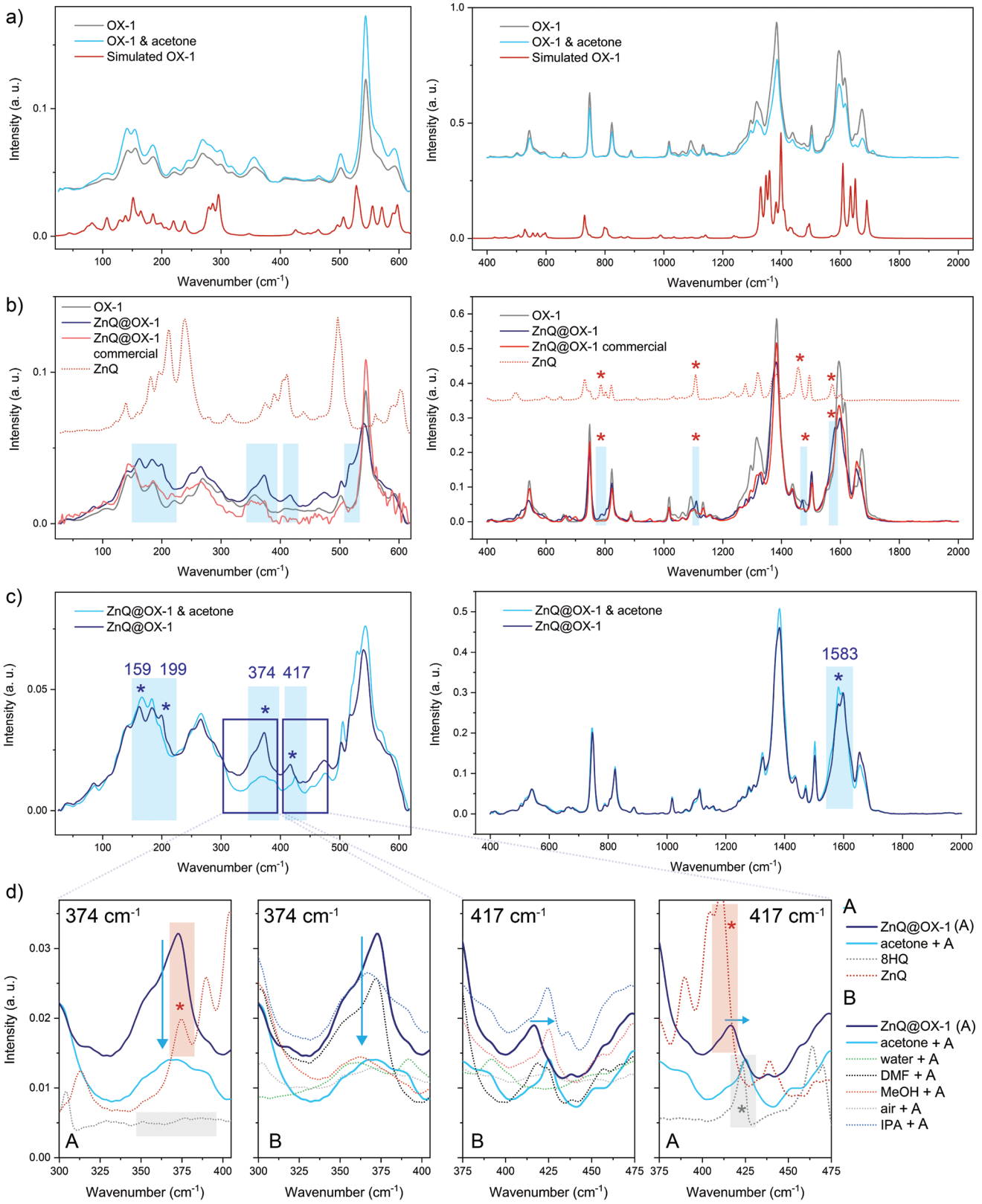

Figure 3. SR-FTIR spectra. a) OX-1 and acetone reveal no spectral changes. b) Simultaneous formation and encapsulation of ZnQ in the OX-1 framework lead to structural and chemical changes that are not observed when commercial ZnQ is added during the synthesis of OX-1 (ZnQ@OX-1 commercial). These chemical interactions are key to the sensing performance. c) Upon exposure to acetone, chemical changes are observed. d) Insets show comparison with pristine guest material and evolution of specific modes upon exposure to various solvents.

complex, and solvents, that are key to the sensing performance, while the functional groups of both materials are still intact, as shown in the mid-IR region, where all additional peaks can be explained by the presence of ZnQ (Figure 3b).

Since the simultaneous formation of ZnQ and OX-1 lattice induce a competition for Zn atoms, some 8HQ molecules might be bound to Zn clusters of the framework, or even interacting with the BDC linker and remaining DMF molecules in the axial position. As a result, the confined ZnQ complex is in fact a derivative, where the altered atomic environment leads to different electronic states, and thus distinctive luminescent behavior. This phenomenon can ultimately explain why we observe the blue emission instead of the green emission, which would be characteristic for ZnQ if isolated in the pores of the framework. As soon as the ZnQ@OX-1 complex is exposed to solvents such as acetone, water, or methanol—all of these relatively "small" solvents that can infiltrate the framework through channels and pores—spectral changes are induced, while "larger" solvents (e.g., DMF) do not disrupt the framework (Figure 3c,d, Figures S10 and S11, Supporting Information), as they do not enter in the pores.

We also probed derivatives of the ZnQ@OX-1 system (8HQ@OX-1, commercial ZnQ@OX-1), exposed to acetone and other solvents, and yet, only the ZnQ@OX-1 complex, as synthesized in a one-pot reaction, exhibited a visible response. Even though small spectral changes can be observed if 8HQ@OX-1 is exposed to acetone, an observation which we attribute to the coordination of some 8HQ molecules to the Zn clusters of OX-1 (and de facto forming ZnQ complexes), their concentration is still too small to produce an emissive material. Therefore, neither a visible change in color nor any optochemical response can be observed for 8HQ@OX-1 as opposed to the ZnQ@OX-1 system. The sensing mechanism of the latter is better understood through a closer look at the spectral changes happening in the presence of acetone. For instance, upon exposure, the peak at 169 cm^{-1} shifts back to a lower energy at 158 cm^{-1}, a peak that is linked with O—Zn—O wagging and ring torsion in pristine OX-1. Similarly, the intensity of the additional peak at 199 cm^{-1}, only observed after guest confinement and attributed to the CH_3 rocking and C–O–Zn rocking in ZnQ, is reduced (Figure 3c). This almost indicates that the framework "recovers" when small solvents enter the framework and disrupt the host–guest interactions between ZnQ and OX-1. The intensity of the peak at 374 cm^{-1}, which is only observed in ZnQ@OX-1 and can be attributed to the vibrations of the Zn—O bonds in ZnQ, decreases when the material is exposed to acetone, or other small solvents, whereas less pronounced changes to this vibrational band are exhibited in the presence of the larger 2-propanol (IPA) molecules, as, due to their size, they will infiltrate the framework at a slower rate (Figure 3d). No changes are observed when the material is exposed to DMF, as remaining solvent molecules are likely to be present in the framework after synthesis. It is worth noting that this peak is absent in the 8HQ molecule without coordination to Zn clusters.

The above finding leads to the conclusion that, upon exposure to small solvents (e.g., water, MeOH, and acetone), the host–guest interactions are disrupted as the solvent molecules enter the framework, and as a result, the guest interacts with the solvent rather than the framework. Now, the Zn—O and Zn—N interactions of the guest that is partially bound to the framework, with the zinc atom initially connected to one quinoline molecule and the framework on the other coordination site, are disturbed, and the guest is not fully coordinated to the framework anymore. The same is true for the peak at 417 cm^{-1}, which, too, is attributed to Zn—O modes in ZnQ. When exposed to acetone or methanol, this peak is shifted to 425 cm^{-1}, a mode associated with 8HQ (Figure 3d). Akin to the previous explanation, the solvent molecules interrupt the interactions between ZnQ and OX-1, and the confined ZnQ complex is not coordinated with the framework anymore. Instead, the spectral fingerprint of the framework is more similar to pristine OX-1, and a mix of conventional ZnQ and 8HQ molecules is prevalent. If the ZnQ@OX-1 system is exposed to acetone or methanol, this phenomenon, coupled with the possibility of guest aggregation, can also explain the observed decrease and shift in emission intensity to the one expected for undistorted ZnQ.

2.3. In Situ Gas Dosing Experiments with Synchrotron-Based FTIR Spectroscopy

While these findings explain the sensing mechanisms, we now turn to the open questions on the level of detection and reversibility of the sensing itself. Again, we employed SR-FTIR, albeit operated with a Harrick flow cell, where small amounts of acetone were injected into dry nitrogen carrier gas. One useful assumption to make is that all the liquid acetone injected into the system vaporizes and passes through the sample cell, although some trace amounts are likely to remain on the metal surfaces of the pipes leading up to the sample cell. For a first approximation, this assumption allows for a calculation of acetone concentration: if the total volume under the surface of the time-resolved acetone vapor spectra corresponds to the amount of acetone injected, then the volume element at any point in time under these spectra corresponds to a proportional fraction of the total volume of acetone injected. Integration over the entire spectrum at a specific time then provides the acetone concentration in the sample cell at that time step (**Figure 4**a–c). The injected volume was altered between 1 and 50 µL, and yet, the maximum concentration of acetone in the cell remained under 8 g L^{-1} or 0.8% of cell volume (Figure 4c). There is no doubt that additional peaks at 392, 492, 529, 1220, 1358, and 1710 cm^{-1} can be observed when acetone reaches the pristine OX-1 sample (Figure 4d). But while this is true, all these peaks can directly be assigned to the peaks of acetone, indicating the lack of chemical interactions between the sample and volatile gas. As expected, the injection of higher amounts of acetone (10, 20, and 30 µL) leads to stronger occurrence of the corresponding peaks, while the recurrent injection of 30 µL demonstrates reversibility of the measurement, although some acetone is deemed to remain on the surface of the cell (Figure 4d).

The optochemically responsive ZnQ@OX-1 complex, in turn, exhibits strong spectral changes upon gas dosing with acetone. As little as 5 µL (or 1.5 g L^{-1} in the sample cell) is enough for the material's response to be detected in the FTIR spectrum (**Figure 5**b). To some extent, the responsiveness scales with the

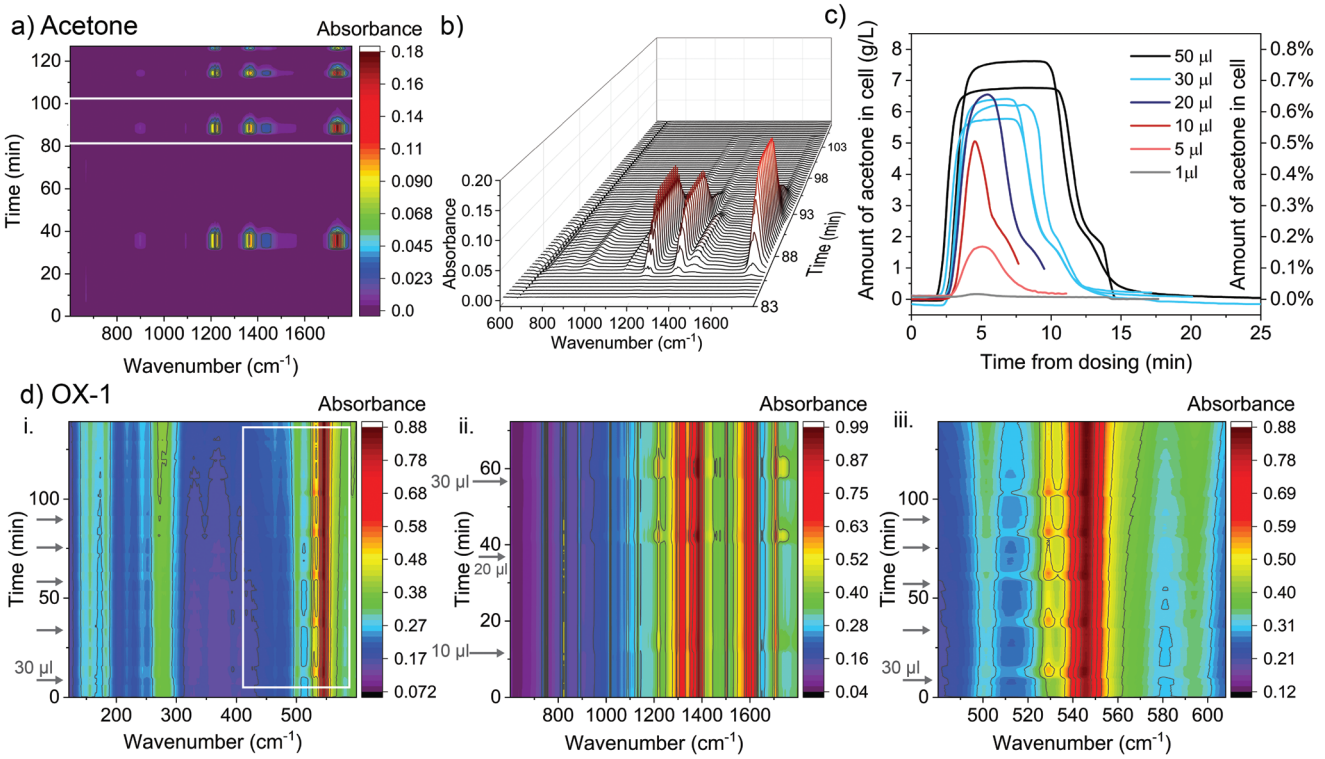

Figure 4. Reference measurements for gas dosing experiments with SR-FTIR. a) Time-resolved spectra of flow cell exposed to N_2 carrier gas with acetone injections. b) 3D plot of transient spectra corresponding to the second injection. At $t = 100$ min, the flow rate was increased to flush the remaining acetone. c) Calculated acetone concentration in cell after injections. d) OX-1 exposed to acetone injections: i) far-IR spectrum, 5 times injected with 30 µL, ii) mid-IR spectrum, injected with 10, 20, and 30 µL, iii) Mid-IR spectrum injected with 5×30 µL.

amount of acetone injected, although the system seems to be saturated after high injections and irreversible changes in the spectrum appear. On the question of reversibility, we repeatedly injected 30 µL into the system, and the response is clearly reversible, however, the same trend that large amounts of acetone induce permanent changes in the framework eventually reduce the sensing ability of the material (Figure 5c). As discussed before, the key vibrational band at 169 cm^{-1}, associated with Zn—O wagging and ring torsion in OX-1, is shifted, and the peak at 199 cm^{-1} that has emerged after guest encapsulation is strongly reduced when exposed to acetone (Figure 5d-i). Similarly, the peak at 374 cm^{-1} (Zn—O) decreases, even permanently, and does not recover. An additional peak emerges at 439 cm^{-1}, and the peak at 417 cm^{-1} is shifted to higher energies, indicating that Zn—O bonds are replaced with O—H bonds, as the interactions between the solvent and ZnQ substitute the host–guest interactions (Figure 5d-ii). Turning to the mid-IR region, we observe an increase of the vibrations around 1710 cm^{-1} that are related to the presence of acetone. Interestingly, the linker vibrations at 1582 and 1654 cm^{-1}, both initially decreased and shifted to lower wavenumber when ZnQ is encapsulated, are now subject to changes in intensity and shifted in wavelengths, respectively, while ring modes (such as 1494 cm^{-1}) neither change upon guest encapsulation nor in the presence of acetone (Figure 5d-iii). The main difference lies in the functional groups that are involved: it is mainly the modes associated with the C and O atoms of the linker that are affected by host–guest and solvent interactions rather than the aromatic rings. More specifically, the intensity of the peak at 1654 cm^{-1} (or 1737 cm^{-1} in the unscaled DFT simulation) that is associated with the twisting mode of the O—C—O groups is strongly decreased in the presence of acetone or methanol. The peak at 1494 cm^{-1} (≈1567 cm^{-1} in DFT simulated spectrum), in contrast, is attributed to CH rocking and in-phase ring mode, and thus hardly affected. This is an indicator that ZnQ interacts with both the O atoms in the linker and the Zn clusters, but not with the aromatic ring itself. Similarly, the ring of the ZnQ molecule is unaffected by host–guest interactions, as confirmed by DFT calculations, where two different models were simulated (Figure S18, Supporting Information). Hence, the strong interactions between the Zn and O atoms of the linker, Zn clusters, ZnQ, and DMF that result in a distorted framework and an altered ZnQ complex, hold the key to the extremely sensitive behavior, and the ability to sense volatile acetone, which further relies on the ability of small solvent molecules to enter the framework and disrupt bespoke interactions.

2.4. Fluorescence Spectroscopy and In Situ Gas Dosing with Near-Field Infrared Spectroscopy

The foregoing findings, which in fact suggest that even low amounts of volatile acetone can lead to an optochemical response of the ZnQ@OX-1 complex, motivated us to perform gas dosing experiments with fluorescence spectroscopy, since changes in emission can be detected more easily than

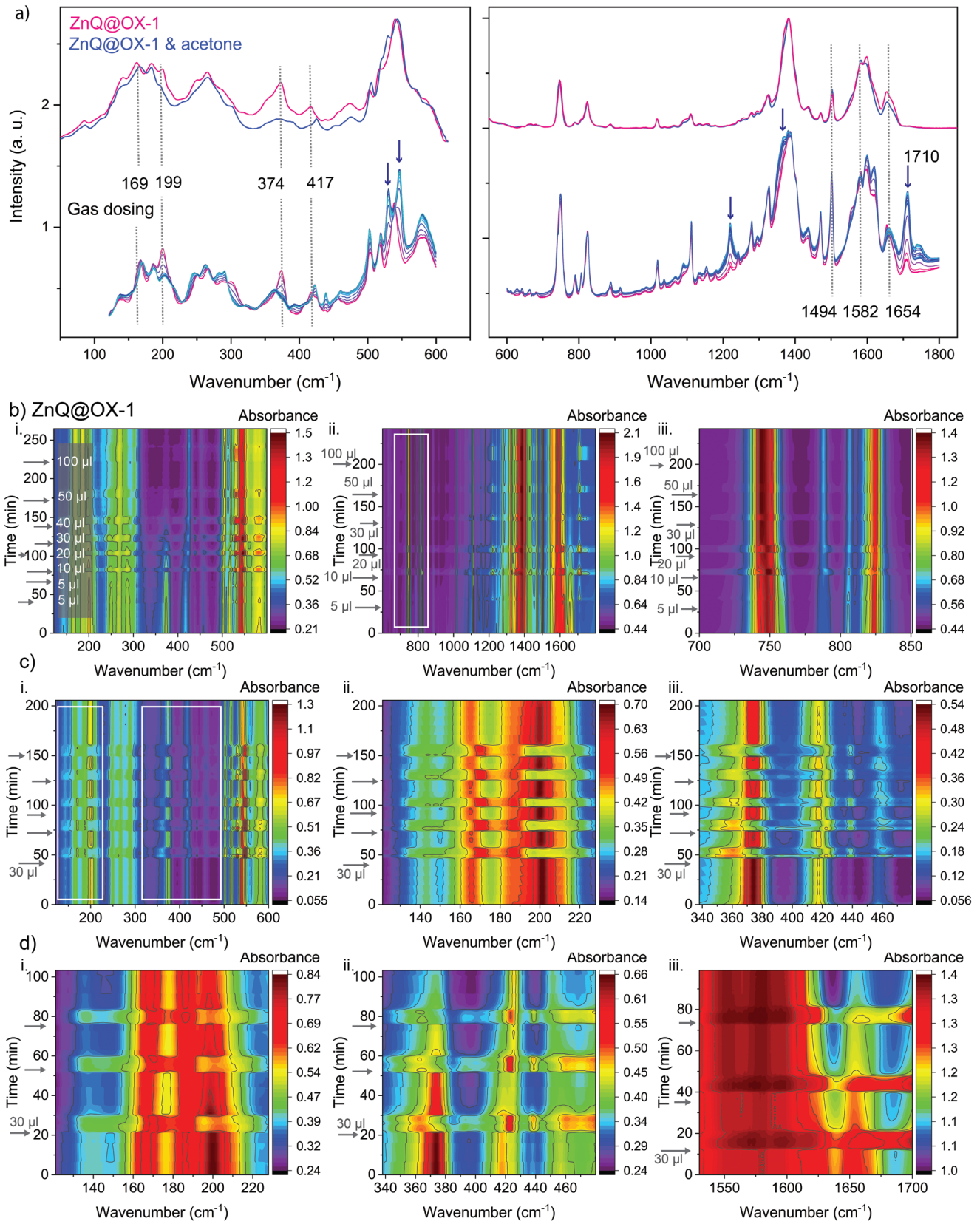

Figure 5. Gas dosing experiments of ZnQ@OX-1 with SR-FTIR. a) SR-FTIR absorption spectra of ZnQ@OX-1 before and after exposure to acetone compared with in situ gas dosing measurements using transmission SR-FTIR. b) Contour plots showing time-dependent spectral data of ZnQ@OX-1 exposed to increasing amounts of acetone (i. far-IR, ii. mid-IR, iii. Zoomed into region 700–850 cm^{-1}). c) ZnQ@OX-1 exposed to 5 injections of 30 µL (i. far-IR, ii. 120–230 cm^{-1}, iii. 340–500 cm^{-1}). d) ZnQ@OX-1 exposed to 3 × 30 µL.

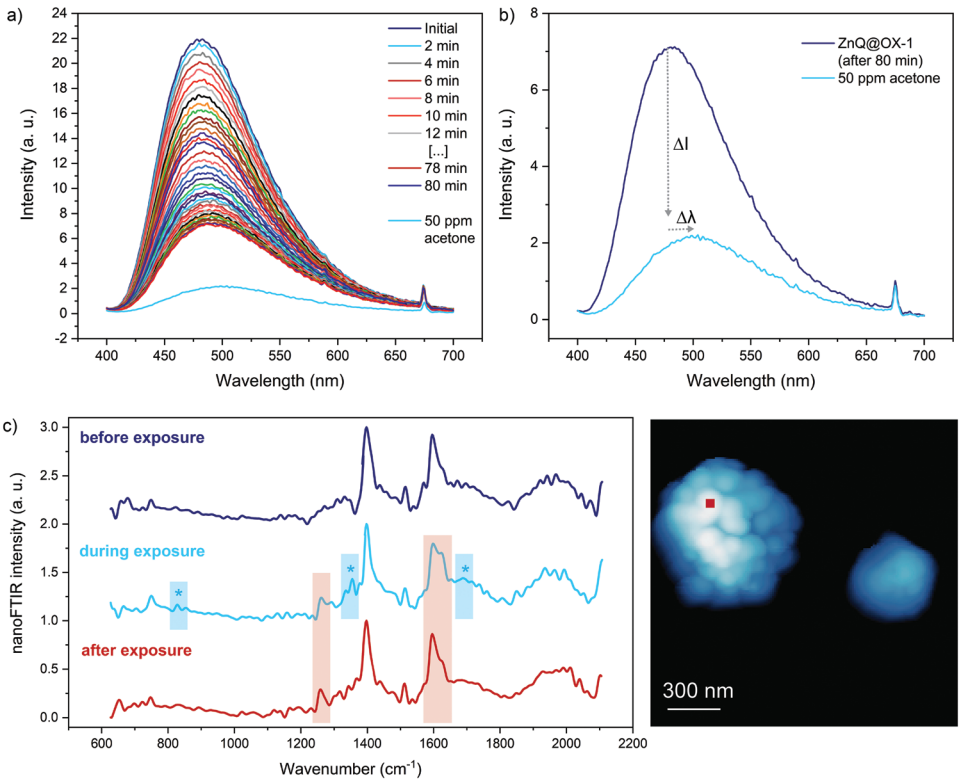

Figure 6. Response of ZnQ@OX-1 to low concentrations of acetone. a) Emission spectra of ZnQ@OX-1 after exposure to air. b) Emission spectra of ZnQ@OX-1 after 80 min (stable emission) and exposed to 50 ppm volatile acetone. c) Near-field infrared spectroscopy on a 20 nm spot on individual crystals of ZnQ@OX-1 before, during and after exposure to acetone (position indicated in AFM image).

chemical transformations in FTIR spectroscopy. In the light of this, we employed a fluorescence spectrometer with a customized gas flow cell to dose the sample with acetone concentrations as low as 5 ppm (see Figure S3, Supporting Information). Prior to dosing, a strong decrease in emission intensity is observed; a trend that we attribute to the initial "activation" of the pristine material (Figure 5a). Either it is the photo-instability induced by the strong emission of the Xenon lamp, or the sensitivity to the humidity of ZnQ@OX-1 in the presence of ambient air. The latter seems to be more likely, especially, since we performed the same experiment without intermediate steps to avoid illumination of the sample, and the same decrease in intensity with time was observed. Nevertheless, after 60 min, the change in emission intensity has stagnated. With this stability being attained, a low concentration of acetone (e.g., 50 ppm) was then injected into the closed system, and vaporized in a round-bottom flask heated at 50 °C before reaching the sample cell through pipes. Interestingly, even such low concentrations of acetone vapor, lead to the shift in emission from 480 to 510 nm, coupled with a strong quenching of emission (**Figure 6**a,b). An irreversible response is however observed if larger amounts of acetone are adsorbed by the sample.

To push the limit of detection even further, we used nanoscale analytical techniques to show in situ gas adsorption from a new perspective: at the single-crystal level. Herein, scattering-type scanning near-field optical microscopy (s-SNOM) in combination with nano-FTIR allowed us to measure the IR spectrum of a 20 nm spot on the ZnQ@OX-1 crystal.[35–37] We then exposed the crystal to acetone vapor by placing an open vial with liquid acetone in proximity to the measurement stage. During the measurement, the acetone evaporates and reaches the ZnQ@OX-1 sample. Interestingly, as shown in Figure 6c, we observe the same spectral changes from a single crystal when compared with "bulk" measurements performed on polycrystalline samples in the order of milligrams (conventional FTIR techniques, fluorescence spectroscopy) to grams (INS). More specifically, only during exposure, the acetone peaks at 1358 and 1710 cm^{-1} emerge in the nano-FTIR spectrum and disappear again, while the acetone-induced chemical changes in the framework, such as the substitution of Zn—O bonds (indicated by the peak at 1654 cm^{-1}) and DMF molecules, are even detectable after exposure. This first exemplar of in situ gas adsorption on single crystal not only demonstrates a new nanoscopic route to study sensing phenomena on much smaller scales, but also unveils the strong response of ZnQ@OX-1 to acetone vapor.

3. Conclusion

In summary, we performed an in depth and multimodal study on the unique sensing behavior of ZnQ@OX-1, which exhibits a visible luminescent color change when exposed to small amounts of volatile acetone. Using high-resolution spectroscopy techniques based on INS and SR-FTIR revealed that the OX-1 framework changes when ZnQ is encapsulated in a one-pot synthetic route. Corresponding DFT simulations explained

the empirically shown vibrational changes and provided further insights into the sensing mechanism: during the synthesis, the interaction with DMF solvent molecules and the competition for Zn clusters between the formation of OX-1 and ZnQ led to a distorted framework and a derivative ZnQ complex exhibiting different luminescent behavior when compared to ZnQ either in solution or aggregates (see Figure S15 in the Supporting Information). Upon exposure to acetone, or other small molecule solvents, the host–guest interactions are disrupted and ZnQ returns to its normal state, as revealed by the green emission that is expected when ZnQ is isolated in the pores of OX-1. Using in situ gas dosing experiments with synchrotron radiation, we observed a reversible response, although large amounts of acetone led to irreversible changes. To push the limit of detection, we further employed fluorescence spectroscopy, where amounts as low as 50 ppm of acetone resulted in the quenching and shift in emission. In addition, we achieved the first in situ gas adsorption on single-crystals using near-field infrared nanospectroscopy, which reveal the same spectral changes as observed with conventional FTIR techniques. We found that ZnQ@OX-1 is unstable in water vapor and therefore, the design of a sensing device focusing on human breath needs further development to shield the active material from water-induced degradation (e.g., encapsulation in a hydrophobic polyvinyl difluoride (PVDF) matrix). Our findings explain the underlying mechanism of the exceptional sensing behavior of ZnQ@OX-1 that was previously unknown. Ultimately, this understanding can be leveraged to tune the system further and achieve better stability while maintaining the high-sensitivity sensing performance.

Supporting Information

Supporting Information is available from the Wiley Online Library or from the author.

Acknowledgements

A.F.M. thanks the Oxford Ashton Memorial Scholarship for a D.Phil. studentship award. J.-C.T. and A.F.M. are grateful for funding through the ERC Consolidator Grant (771575 (PROMOFS)) and the EPSRC Impact Acceleration Account Award (EP/R511742/1). The authors are grateful for large facilities access through the ISIS Beamtime at TOSCA (RB2010346) and the Diamond Beamtime at B22 MIRIAM (SM14902-3 and SM25407-2). The authors acknowledge the use of the University of Oxford Advanced Research Computing (ARC) facility in carrying out this work (https://doi.org/10.5281/zenodo.22558). Via the membership of the U.K.'s HEC Materials Chemistry Consortium (MCC), which is funded by EPSRC (EP/R029431), this work used the ARCHER2 UK National Supercomputing Service (http://www.archer2.ac.uk).

Conflict of Interest

The authors declare no conflict of interest.

Data Availability Statement

The data that support the findings of this study are available from the corresponding author upon reasonable request.

Keywords

gas dosing, inelastic neutron scattering, infrared spectroscopy, metal-organic frameworks, sensing mechanism

Received: June 23, 2022
Revised: September 13, 2022
Published online:

[1] L. E. Kreno, K. Leong, O. K. Farha, M. Allendorf, R. P. Van Duyne, J. T. Hupp, *Chem. Rev.* **2012**, *112*, 1105.
[2] G. Matzeu, L. Florea, D. Diamond, *Sens. Actuators, B* **2015**, *211*, 403.
[3] M. Phillips, J. Herrera, S. Krishnan, M. Zain, J. Greenberg, R. N. Cataneo, *J.Chromatogr. B: Biomed. Sci. Appl.* **1999**, *729*, 75.
[4] J. D. Fenske, S. E. Paulson, *J. Air Waste Manage. Assoc.* **1999**, *49*, 594.
[5] S. Das, M. Pal, *J. Electrochem. Soc.* **2020**, *167*, 037562.
[6] I. Stassen, N. Burtch, A. Talin, P. Falcaro, M. Allendorf, R. Ameloot, *Chem. Soc. Rev.* **2017**, *46*, 3185.
[7] H. Furukawa, K. E. Cordova, M. O'Keeffe, O. M. Yaghi, *Science* **2013**, *341*, 1230444.
[8] Z. Hu, B. J. Deibert, J. Li, *Chem. Soc. Rev.* **2014**, *43*, 5815.
[9] W. Li, X. Wu, N. Han, J. Chen, X. Qian, Y. Deng, W. Tang, Y. Chen, *Sens. Actuators, B* **2016**, *225*, 158.
[10] W. Li, X. Wu, N. Han, J. Chen, W. Tang, Y. Chen, *Powder Technol.* **2016**, *304*, 241.
[11] E. Cao, Z. Guo, G. Song, Y. Zhang, W. Hao, L. Sun, Z. Nie, *Sens. Actuators, B* **2020**, *325*, 128783.
[12] J. Xia, K. Diao, Z. Zheng, X. Cui, *RSC Adv.* **2017**, *7*, 38444.
[13] F. Gu, H. Chen, D. Han, Z. Wang, *RSC Adv.* **2016**, *6*, 29727.
[14] I. Ellern, A. Venkatasubramanian, J. H. Lee, P. J. Hesketh, V. Stavila, M. D. Allendorf, A. L Robinson, *ECS Trans.* **2013**, *50*, 469.
[15] S. Homayoonnia, S. Zeinali, *Sens. Actuators, B* **2016**, *237*, 776.
[16] P. Ju, H. Yang, L. Jiang, M. Li, Y. Yu, E. Zhang, *Spectrochim. Acta, Part A* **2021**, *246*, 118962.
[17] F. Klongdee, S. Youngme, J. A. L. Boonmak, *Polyhedron* **2020**, *180*, 114437.
[18] L. Bai, A. Jana, H. P. Tham, K. T. Nguyen, P. Borah, Y. Zhao, *Small* **2016**, *12*, 3302.
[19] A. K. Chaudhari, H. J. Kim, I. Han, J. C. Tan, *Adv. Mater.* **2017**, *29*, 1701463.
[20] T. Tsuboi, Y. Nakai, Y. Torii, *Open Phys.* **2012**, *10*, 524.
[21] H. Jianbo, Z. Tingting, C. Yongjing, Z. Yuanyuan, Y. Weiqing, M. Menglin, *J. Fluoresc.* **2018**, *28*, 1121.
[22] G. Mehlana, S. A. Bourne, *CrystEngComm* **2017**, *19*, 4238.
[23] Y. Li, A.-S. Xiao, B. Zou, H.-X. Zhang, K.-L. Yan, Y. Lin, *Polyhedron* **2018**, *154*, 83.
[24] D. Colognesi, M. Celli, F. Cilloco, R. J. Newport, S. F. Parker, V. Rossi-Albertini, F. Sacchetti, J. Tomkinson, M. Zoppi, *Appl. Phys. A* **2002**, *74*, s64 .
[25] R. Dovesi, V. R. Saunders, C. Roetti, R. Orlando, C. M. Zicovich-Wilson, F. Pascale, B. Civalleri, K. Doll, N. M. Harrison, I. J. Bush, P. D'Arco, M. Llunell, M. Causà, Y. Noël, L. Maschio, A. Erba, M. Rerat, S. Casassa, *CRYSTAL17 User's Manual.*, University of Torino, Torino **2017**.
[26] R. Dovesi, R. Orlando, A. Erba, C. M. Zicovich-Wilson, B. Civalleri, S. Casassa, L. Maschio, M. Ferrabone, M. De La Pierre, P. D' Arco, Y. Noël, M. Causà, M. Rérat, B. Kirtman, *Int. J. Quantum Chem.* **2014**, *114*, 1287.
[27] L. Dona, J. G. Brandenburg, I. J. Bush, B. Civalleri, *Faraday Discuss.* **2020**, *224*, 292.
[28] L. Dona, J. G. Brandenburg, B. Civalleri, *J. Chem. Phys.* **2022**, *156*, 094706.

[29] A. F. Möslein, L. Donà, B. Civalleri, J.-C. Tan, *ACS Appl. Nano Mater.* **2022**, *5*, 6398.
[30] B. E. Souza, L. Dona, K. Titov, P. Bruzzese, A. S. Babal, A. F. Möslein, M. D. Frogley, G. Wolna, G. Cinque, B. Civalleri, J. C. Tan, *ACS Appl. Mater. Interfaces* **2020**, *12*, 5147.
[31] T. Xiong, Y. Zhang, L. Donà, M. Gutiérrez, A. F. Möslein, A. S. Babal, N. Amin, B. Civalleri, J.-C. Tan, *ACS Appl. Nano Mater.* **2021**, *4*, 10321.
[32] M. R. Ryder, B. Civalleri, G. Cinque, J.-C. Tan, *CrystEngComm* **2016**, *18*, 4303.
[33] M. R. Ryder, B. Civalleri, T. D. Bennett, S. Henke, S. Rudic, G. Cinque, F. Fernandez-Alonso, J. C. Tan, *Phys. Rev. Lett.* **2014**, *113*, 215502.
[34] J. Maul, M. R. Ryder, M. T. Ruggiero, A. Erba, *Phys. Rev. B* **2019**, *99*, 014102.
[35] F. Huth, A. Govyadinov, S. Amarie, W. Nuansing, F. Keilmann, R. Hillenbrand, *Nano Lett.* **2012**, *12*, 3973.
[36] B. Knoll, F. Keilmann, *Nature* **1999**, *399*, 134.
[37] A. F. Möslein, M. Gutierrez, B. Cohen, J. C. Tan, *Nano Lett.* **2020**, *20*, 7446.